Optics Communications 507 (2022) 127661

Contents lists available at ScienceDirect

Optics Communications

journal homepage: www.elsevier.com/locate/optcom

Uniform rectangular distribution of far-field intensity by optical phased array

Lanxuan Zhang [a], Yubing Wang [b], Yu Hou [a], Junfeng Song [a,c,*]

[a] State Key Laboratory of Integrated Optoelectronics, College of Electronic Science and Engineering, Jilin University, 2699 Qianjin Street, Changchun, 130012, China

[b] State Key Laboratory of Luminescence and Application, Changchun Institute of Optics, Fine Mechanics and Physics, Chinese Academy of Sciences, Changchun, 130010, China

[c] Peng Cheng Laboratory, Shenzhen, 518000, China

ARTICLE INFO

Keywords:
Optical phased array
Uniform rectangular distribution
Flash Lidar

ABSTRACT

In this paper, to solve the problem of uneven distribution of far-field intensity of Flash Lidar, a method of amplitude modulation for optical phased array (OPA) is proposed, which makes the far-field intensity distribution close to the uniform rectangular distribution. We use the impulse response sequence of Finite Impulse Response (FIR) digital filter designed by the window functions to modulate the amplitude of the OPA. This kind of uniform intensity distribution can simultaneously detect a wide range with the same intensity. The modulation sequence can also be extended to two-dimensional situation. In the case of considering the radiation pattern of optical waveguide, the amplitude modulation sequence can also be modified to obtain the far-field pattern that is close to the uniform rectangular distribution.

1. Introduction

Compared with traditional microwave radar, the laser emitted by Lidar (Light Detection and Ranging) has the characteristics of high brightness, high directivity, high monochromaticity and high coherence. Lidar has the high angular resolution, high range resolution [1], high speed resolution, wide speed range and strong anti-interference ability. Because of the advantages of Lidar, it has broad application prospects: future airborne Lidar, vehicle-borne Lidar, and intelligent robots, especially in traffic control, target tracking, automatic driving in intelligent cities.

Lidar is divided into mechanical Lidar and solid-state Lidar, traditional mechanical scanning Lidar is composed of discrete optoelectronic devices, optical components and electronic components. It is difficult to realize mass production because of its large size, low reliability and high cost [2], so the solid-state Lidar has become the mainstream research because of its high integration, small size, high reliability and low cost.

Flash Lidar is a very important branch of solid-state Lidar [3,4]. Instead of scanning, it emits a large area of laser covering the detection area in a short time, and then receives it with a highly sensitive receiver to complete the rendering of the surrounding image [5]. Flash Lidar is a promising technology. National Aeronautics and Space Administration (NASA) recognizes the Flash Lidar technology as an important tool for enabling safe and precision landing in future unmanned and crewed lunar and planetary missions [6]. Flash Lidar is selected to accomplish Autonomous Landing and Hazard Avoidance Technology (ALHAT) Project of accurate landing at the selected safe site [7]. Flash Lidar can provide 3D point-cloud data in real time without motion blur, in the day or night, and is capable of imaging through fog and clouds [8]. It also has applications in military imaging [9], Unmanned Aerial Vehicle (UAV) surveillance [10] and traffic control [11].

However, the far-field intensity of the laser emitted by the Flash Lidar shows the Gaussian distribution. As shown in Fig. 1(a). The distribution of light field is nonuniform, and the intensity of the edge is weaker than that of the center. Flash Lidar needs to analyze the light reflected from the object, if the intensity at the edge is too weak to be detected by the receiver when it is reflected, this will lead to false imaging, that is we do not want to get.

Therefore, the ideal light intensity situation is a uniform rectangular distribution as shown in Fig. 1(b), in this way the Lidar will avoid the wrong image analysis of the reflected light due to the uneven light intensity. Based on the above problems, we propose a method to realize uniform rectangular far-field intensity distribution by using another solid-state Lidar: optical phased array. The amplitude of the uniform OPA in equal spacing is modulated by the impulse response sequence of the FIR digital filter which is designed by different window functions in the field of digital signal processing, this method makes the far-field pattern of the OPA close to the uniform rectangular distribution.

* Corresponding author at: State Key Laboratory of Integrated Optoelectronics, College of Electronic Science and Engineering, Jilin University, 2699 Qianjin Street, Changchun, 130012, China.

E-mail address: songjf@jlu.edu.cn (J. Song).

https://doi.org/10.1016/j.optcom.2021.127661
Received 29 September 2021; Received in revised form 11 November 2021; Accepted 13 November 2021
Available online 26 November 2021

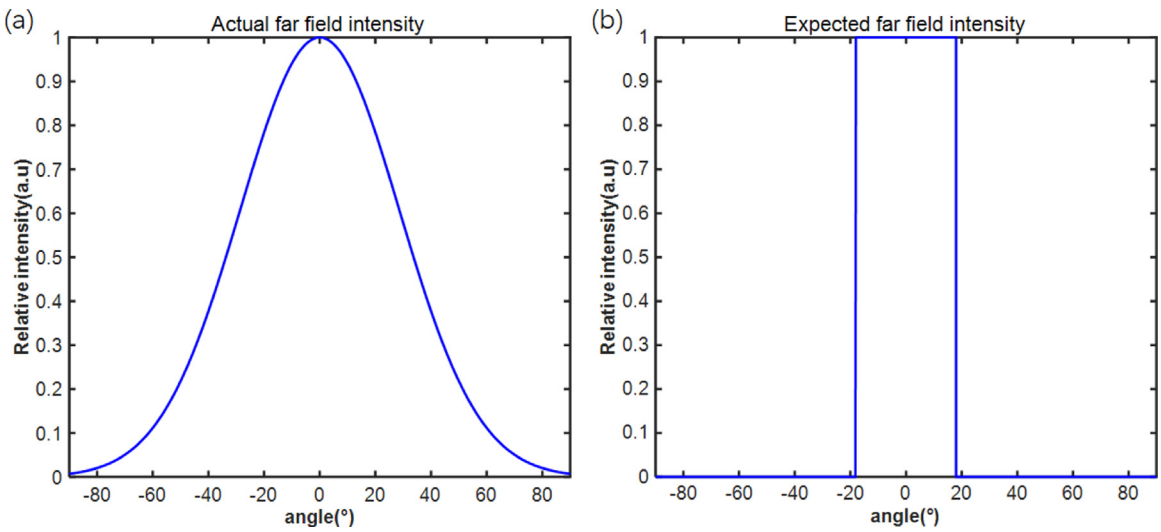

Fig. 1. (a) The actual far-field intensity distribution of the Flash Lidar. The far field intensity presents the Gaussian distribution. (b) The ideal uniform rectangular far field intensity distribution for detection.

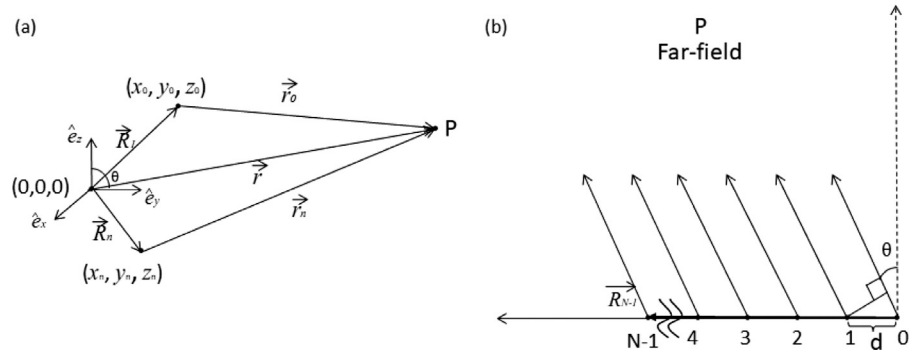

Fig. 2. (a) The geometric model of non-uniform optical phased array. (b) The geometric model of uniformly distributed optical phased array in equal spacing.

2. Realization of far-field intensity rectangular distribution

2.1. OPA geometric model

OPA is a kind of beam pointing control technology [12–23], each waveguide in the OPA is equivalent to a slit in multi-slit interference. Light propagates in the air and interferes. As a result, the energy of the light is enhanced by the interference in one direction, and weakened in another direction, and achieve the purpose of changing the direction of the beam. Fig. 2(a) shows the geometric basic model of an OPA with non-uniformly placed elements. The model ignores the physical size of the elements, assumes that the width of each waveguide is infinitely small. Let the position coordinate of any element be (x_n, y_n, z_n) relative to the phase reference point (0, 0, 0). First of all, considering a single element (x_0, y_0, z_0), at the far field observation point P, the distance between them is r_0, its diffraction field intensity $E_0(P)$ is:

$$E_0(P) = A_0 \exp(j\varphi_0) \frac{\exp(jkr_0)}{r_0} f(\theta) \tag{1}$$

where θ is the diffraction angle, λ is the wavelength, k is the wave-vector and equal to $2\pi/\lambda$, A_0 is the amplitude, φ_0 is the phase, $f(\theta)$ is the radiation pattern of this element. Then we consider that the OPA is composed of many radiation sources, because the coordinate of each radiation source is (x_n, y_n, z_n) relative to the phase reference point, as shown in Fig. 2(a), the vector from reference point to the nth radiation source is defined as $\overrightarrow{R_n} = \hat{e}_x x_n + \hat{e}_y y_n + \hat{e}_z z_n$, according to Eq. (1), the diffraction field intensity of each radiation unit at far-field P is:

$$E_n(P) = A_n \exp(j\varphi_n) \frac{\exp(jkr_n)}{r_n} f_n(\theta) \tag{2}$$

where $r_n = |\overrightarrow{r_n}| = \left|\vec{r} - \overrightarrow{R_n}\right| = r\sqrt{1 + \left(x_n^2 + y_n^2 + z_n^2\right)/r^2 - 2\left(xx_n + yy_n + zz_n\right)/r^2}$, replacing rectangular coordinates with spherical coordinates: $x = r\sin\theta\cos\varphi, y = r\sin\theta\sin\varphi, z = r\cos\theta$, and for the far-field:

$$\frac{x_n^2 + y_n^2 + z_n^2}{r^2} = \frac{\left|\overrightarrow{R_n}\right|^2}{r^2} \ll 1 \tag{3}$$

so r_n can be calculated approximately: $r_n = r - (x_n\sin\theta\cos\varphi + y_n\sin\theta\sin\varphi + z_n\cos\theta)$, it can be concluded that the phase contribution of the nth element to the far-field point P is:

$$\exp(jkr_n) = \exp(jkr)\exp\left[-jk\left(x_n\sin\theta\cos\varphi + y_n\sin\theta\sin\varphi + z_n\cos\theta\right)\right] \tag{4}$$

As for vector $\vec{r}$, its unit vector $\overrightarrow{r_e}$:

$$\overrightarrow{r_e} = \frac{\vec{r}}{|\vec{r}|} = \hat{e}_x\sin\theta\cos\varphi + \hat{e}_y\sin\theta\sin\varphi + \hat{e}_z\cos\theta \tag{5}$$

Therefore, Eq. (4) can be written by $\exp(jkr_n) = \exp(jkr)\exp\left[-jk\left(\overrightarrow{R_n}\cdot\overrightarrow{r_e}\right)\right]$. Finally, the field intensity of the nth element at far field P is:

$$E_n(P) = A_n \exp(j\varphi_n) \frac{\exp(jkr)\exp\left[-jk\left(\overrightarrow{R_n}\cdot\overrightarrow{r_e}\right)\right]}{r_n} f_n(\theta) \tag{6}$$

The N-element OPA model with uniformly distributed elements in a straight line is shown in Fig. 2(b), this model also ignores the physical size of each element, assuming that the width of each waveguide is

infinitely small and the spacing of each element is d. The position of the first waveguide is defined as the phase reference point. It can be obtained from geometric relations that $k\left(\overrightarrow{R_n}\cdot\overrightarrow{r_e}\right)=knd\sin\theta$, therefore, in the equidistant OPA, the far-field intensity produced by each element at point P is:

$$E_n(P)=A_n\exp\left(j\varphi_n\right)\frac{\exp(jkr)\exp(-jknd\sin\theta)}{r_n}f_n(\theta) \tag{7}$$

The total intensity at the far-field observation point P can be seen as the superposition of the diffraction photoelectric field at the point P of each element of the one-dimensional OPA, so:

$$E(P)=\sum_{n=0}^{N-1}E_n(P)=\sum_{n=0}^{N-1}A_n\exp\left(j\varphi_n\right)\frac{\exp(jkr)\exp(-jknd\sin\theta)}{r_n}f_n(\theta) \tag{8}$$

If the shape of each phased array element is the same and the radiation pattern is the same, too. The above formula can be written as follows:

$$E(P)=f(\theta)\sum_{n=0}^{N-1}A_n\exp\left(j\varphi_n\right)\frac{\exp(jkr)\exp(-jknd\sin\theta)}{r_n} \tag{9}$$

In Eq. (9), the distance from each phased array element to the far field point P r_n can be approximately regarded as equal to the distance from the reference point to the far-field point r, then:

$$E(P)=f(\theta)\frac{\exp(jkr)}{r}\sum_{n=0}^{N-1}A_n\exp\left[j\left(\varphi_n-knd\sin\theta\right)\right] \tag{10}$$

From the above formula, we can see that $E(P)$ is a function of θ, so it can be expressed as $E(\theta)$. But what we care about is not the absolute size of $E(\theta)$, but the relative distribution of it. Therefore, the constant terms of amplitude and phase are neglected, the far-field intensity distribution function of OPA can be expressed as:

$$E(\theta)=f(\theta)\sum_{n=0}^{N-1}A_n\exp\left[j\left(\varphi_n-knd\sin\theta\right)\right] \tag{11}$$

In the above formula, $\sum_{n=0}^{N-1}A_n\exp\left[j\left(\varphi_n-knd\sin\theta\right)\right]$ is the array factor, therefore, $E(\theta)$ is the product of the radiation pattern and the array factor of the phased array. It is assumed that the radiation patterns of all phased array elements are $f(\theta)$=1, Eq. (11) can be written into:

$$E(\theta)=\sum_{n=0}^{N-1}A_n\exp\left[j\left(\varphi_n-knd\sin\theta\right)\right] \tag{12}$$

Set the phase difference between adjacent phased array elements is $\Delta\varphi$, φ_n=$n\Delta\varphi$, if the phase difference between adjacent waveguides $\Delta\varphi = kd\sin\theta_s$, the main lobe can be scanned to θ_s direction. $E(\theta)$ can eventually be expressed as:

$$E(\theta)=\sum_{n=0}^{N-1}A_n\exp\left[jn\left(kd\sin\theta_s-kd\sin\theta\right)\right] \tag{13}$$

Among them, $kd\sin\theta_s$ is the phase difference between adjacent waveguides needed to realize the scanning angle θ_s of the beam, which is called "Phase difference in the array", and $kd\sin\theta$ is called "Phase difference in the space" because of the spatial position distribution of adjacent elements of the phased array.

2.2. Amplitude modulation of uniformly distributed optical phased array

In order to get the ideal uniform far-field pattern, we must design the optical phased array so that the far-field intensity can be uniformly gathered to the central position. In order to achieve this, amplitude modulation must be carried out [19,24], there are many sequences that can be used to modulate the amplitude of an OPA. We use the impulse response sequence of FIR digital filter designed by the window function $\omega(n)$ to modulate the amplitude of the OPA, that is: using different window functions $\omega(n)$ [25] to intercept the infinite impulse response sequence of low pass filter $h_d(n)$ whose cut-off frequency is ω_c to get the sequence $h(n)$ [26]:

$$h(n)=h_d(n)w(n)=\frac{\sin\left[w_c(n-a)\right]}{\pi(n-a)}w(n) \tag{14}$$

The window functions $\omega(n)$ we choose include: Boxcar, Hanning, Hamming, Blackman and Kaiser windows, when the amplitude of the optical phased array is weighted by $h(n)$, the far-field pattern similar to the rectangle distribution is obtained.

We choose Boxcar, Hanning, Hamming, Blackman and Kaiser windows to design FIR filters and to modulate the amplitude of OPA using the impulse response of FIR filter. The waveguide spacing of OPA d = 1 μm, and the number of waveguide N = 64, the cut-off frequency of the filter ω_c = 0.3π. It can be seen that the intensity distribution of far-field tends to uniform rectangular distribution after the amplitude modulation. Fig. 3(b) amplifies the distribution of the far-field intensity, and it can be seen more clearly that the uniformity of the far-field intensity distribution is different under different amplitude modulation conditions. After modulation with the sequence of FIR filter designed by Boxcar window, the uniformity of the far-field pattern is the worst and the fluctuation is very strong, the amplitude distribution of the sequence $h_d(n)$ is not changed by using the Boxcar window, it is just simply intercepted, so the far-field pattern shows a relatively large fluctuation, while other window functions change the amplitude of the sequence while intercepting the sequence, so the window function (except the Boxcar window) can reduce the fluctuation of the far-field pattern and increase the uniformity of the far-field intensity distribution. Fig. 3(c) shows the peak side lobe level (PSLL) of the amplitude-modulated OPA with the sequences of FIR filter designed by Boxcar, Hanning, Hamming, Blackman and Kaiser window is −21.20 dB, −44.00 dB, −55.31 dB, −75.23 dB, −55.15 dB respectively, it can be seen that after the amplitude modulation of this method, when the intensity of far-field is uniform, the side lobe is suppressed to a great extent at the same time. It not only achieves the uniform distribution of the intensity of the far field, but also largely restrains the side lobe. In order to measure the similarity between the far-field intensity distribution of the modulated OPA and the ideal uniform rectangular distribution, the mean absolute deviation between the actual distribution and the ideal distribution is calculated. The data of ideal distribution are expressed as: $M = M_n(m_1, m_2, \ldots, m_N)$, the actual distribution of data is as follows: $A = A_n(a_1, a_2, \ldots, a_N)$, here, N is the sampling point of ideal distribution and actual distribution, and the mean absolute deviation formula is:

$$D(A,M)=\frac{1}{N}\sum_{i=1}^{N}\left|a_i-m_i\right| \tag{15}$$

For the far-field intensity distribution, the mean absolute deviation decreases with the increase of number of waveguides as shown in Fig. 4(a), in other words, the similarity between the far-field distribution and the ideal distribution increases with the number of waveguides, the maximum number of waveguides we choose is 64. The more the number of waveguides, the closer to the ideal uniform rectangular distribution. For different modulation modes, with the same number of waveguides, the optical phased array modulated by the sequence of FIR digital filter designed by Kaiser window has the smallest mean absolute deviation, the smallest amplitude offset from the ideal distribution and is nearest to the uniform rectangular distribution. Then, the effect of number of waveguides on the width of main lobe is investigated. Fig. 4(b) shows that the width of the main lobe is very large at first, the far-field pattern does not have the form of rectangular distribution in this case, but the width of the main lobe decreases suddenly with the increase of the number of waveguide elements, because the far-field intensity distribution is changing from non-uniform distribution to rectangular uniform distribution, and then with the increase of the number of waveguide elements, the width of the main lobe increases slowly and gradually becomes stable. With the increase of the number, it has less

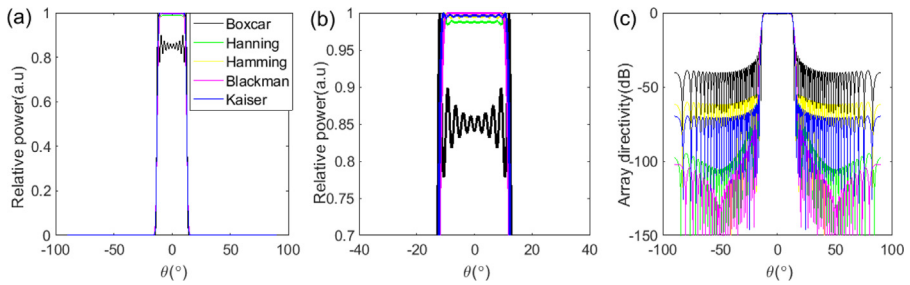

Fig. 3. (a) The far-field intensity distribution of a small-range uniform OPA modulated by impulse response sequences of FIR digital filter designed by five kinds of window functions, the wavelength $\lambda = 1550$ nm. (b) Enlargement of the middle area in Fig. 3(a). (c) The far-field pattern of a small-range uniform optical phased array modulated by the same sequences as Fig. 3(a).

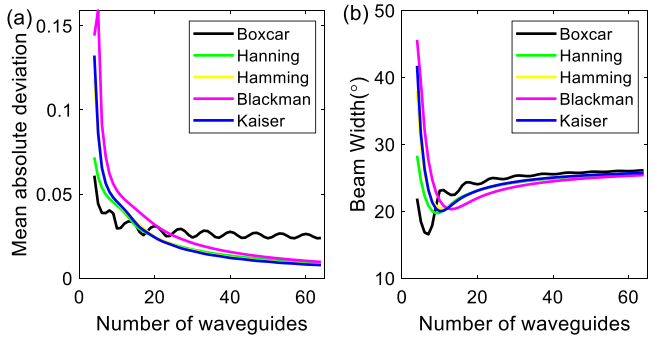

Fig. 4. The performance of far-field pattern of a uniform optical phased array modulated by different sequences. (a) In the case of amplitude modulation with sequences of FIR digital filter designed by five kinds of window functions, the mean absolute deviation is used as the function of the number of waveguides. (b) Beam width is used as the function of the number of waveguides.

and less influence on beam width. From the above analysis, for any amplitude modulation mode, the far-field intensity distribution tends to be more uniform with the increase of the number of waveguides, but the main lobe beam width remains basically unchanged. Visualization 1 records the change of far-field intensity distribution along with the increase of waveguide number.

Let us take impulse response sequence of the FIR filter designed by Kaiser window as an example, investigate the influence of the characteristic of the designed FIR filter on the far-field distribution. Visualization 2 shows that with the increase of the cut-off frequency of the FIR digital filter, the impulse response sequence of the FIR filter designed by Kaiser window also changes, and the amplitude of the center of the sequence increases gradually. The amplitude sequence in two extreme cases is shown in Fig. 5(a). The variation of far-field intensity distribution corresponding to the sequence is also shown in Visualization 2. As shown in Fig. 5(b), the far-field beam width of the uniform optical phased array modulated by the sequence with cut-off frequency of filter is wider than that by the sequence with small cut-off frequency. Fig. 5(c) shows that with the increase of the cut-off frequency of the FIR filter which is designed by Kaiser window for amplitude modulation, the beam width of the far-field intensity distribution increases, when selecting other window functions, the law is the same as that of Kaiser window. All the above analyses are based on element spacing $d = 1$ μm, next, the influence of the waveguide spacing d on the far field pattern is analyzed in the case of the modulation sequence is the sequence of FIR filter designed by Kaiser window. Fig. 6 shows that the far-field pattern of the OPA after amplitude modulation changes with the distance between waveguides when the number of waveguides is 64. Visualization 3 shows the trend of far-field intensity distribution from $d = 0.775$ μm to $d = 3.4$ μm, we can see that with the increase of the waveguide spacing d, the width of the main lobe varies from wide to narrow, then from single lobe to multi-lobe, and the number of grating lobes increases, but the distribution of each grating lobe is approximately rectangular and uniform.

For optical phased array, the main lobe can be pointed to different angles by changing the phase difference between adjacent waveguides. In this paper, the far-field intensity distribution of the small-range uniform optical phased array after amplitude modulation has presented a rectangular uniform distribution, therefore, if the uniform far-field intensity distribution is shifted to another angle, the uniform distribution of the finite width can be filled with the whole detection range and expand the detection range of the Lidar. Fig. 7 shows that the center of the main lobe of the far field intensity distribution which is close to the uniform rectangular distribution is pointing at −30°. Visualization 4 demonstrates the changing process of the far field pattern of the center of the main lobe from −50° to +50°. In this case, the detection range of the uniform far field intensity of the optical phased array exceeds 100°.

When considering the application of the above amplitude modulation to each channel of the actual OPA, due to the limitation of modulation precision, the actual amplitude applied to each waveguide may deviate from the ideal distribution. Let us take impulse response sequence of the FIR filter designed by Kaiser window as an example, investigate the influence of the designed FIR filter sequence with noise on the far-field distribution. We add 10%–50% random noise fluctuation to each group of modulated sequences and calculate the far-fields modulated by them. Fig. 8(a)–(e) show the comparison of the far-fields obtained when noise in different levels is applied to the amplitude modulation sequence and the far-fields corresponding to the sequences without noise. For the noise in different levels, we calculate the mean absolute deviation between the corresponding far-field and the far-field without noise for 100 times and take the average of 100 times as the final result, it is shown in Fig. 8(f). We can see that when 10% noise is applied, the obtained far-field is very close to the original. As the noise in the sequence increases, the mean absolute deviation between the obtained far field and the ideal far field gradually increases, that is, the similarity between them gradually decreases. When 40%–50% noise is applied, undesired side lobes appear in the far field. However, even in this case, the intensity distribution in the main lobe is still maintained above 0.8, which can be approximately regarded as a uniform intensity distribution.

3. Amplitude modulation of two dimensional optical phased array

Two-dimensional optical phased array is the extension of one-dimensional optical phased array. The waveguides arranged in a rectangular grid are called rectangular planar waveguide arrays. As shown in Fig. 9, the geometric model of $M \times N$ two-dimensional optical phased array is located in the x-o-y plane, and the rectangular array can manipulate the beam in the elevation and azimuth directions.

The waveguide spacing in x direction and y direction is d_x and d_y respectively. From the previous analysis, we can see that the intensity of the photoelectric field produced by each radiation element at the far-field P can be calculated by the Eq. (6) derived above. For the vector

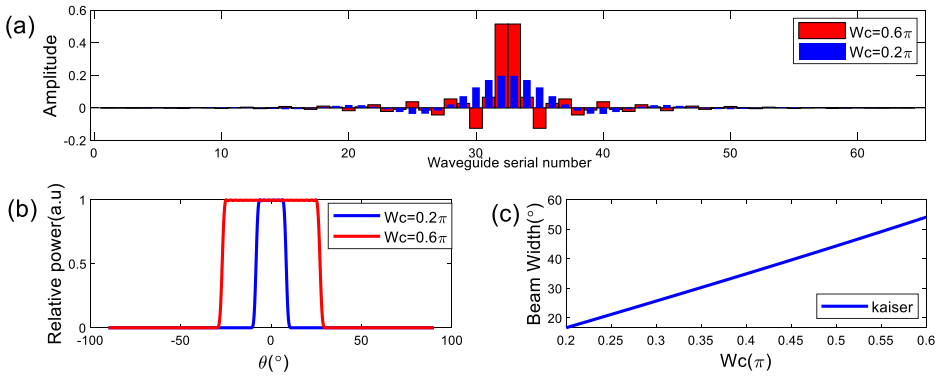

Fig. 5. The influence of the parameter of the FIR filter designed by window functions on the far field intensity distribution, because the impulse response sequence of FIR digital filter with different cut-off frequencies is distinguishing. (a) The impulse response sequence of the FIR filter designed by the Kaiser window, the cut-off frequencies of the FIR filters are 0.2π and 0.6π, respectively. (b) The far-field intensity distribution of the optical phased array after amplitude modulation with the two sequences shown in (a), (c) The beam width as a function of the filter cut-off frequency, when the FIR filter is designed by Kaiser window.

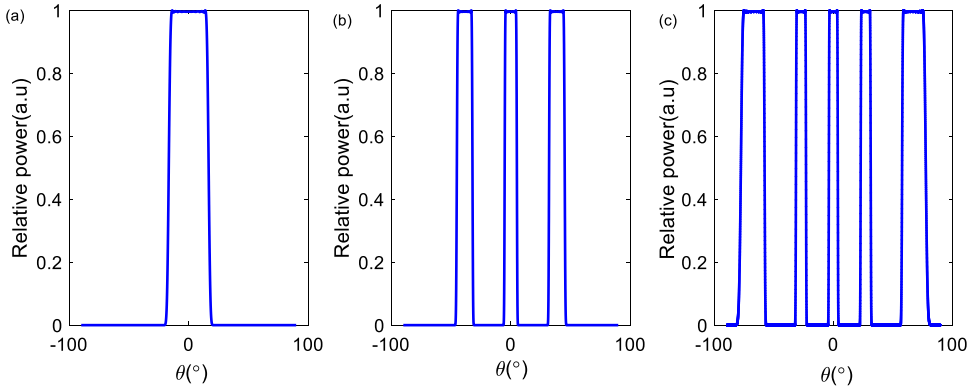

Fig. 6. The far-field pattern of the OPA with different waveguide spacing under the same amplitude modulation, the number of waveguides is 64, wavelength $\lambda = 1550$ nm. (a) When the waveguide spacing $d = 0.775$ μm, the far-field pattern of optical phased array modulated with sequence of FIR filter designed by Kaiser window . (b) When the waveguide spacing $d = 2.5$ μm, the far-field pattern of optical phased array modulated with sequence of FIR filter designed by Kaiser window. (c)When the waveguide spacing $d = 3.4$ μm, the far-field pattern of optical phased array modulated with sequence of FIR filter designed by Kaiser window. The cut-off frequency of the FIR digital filter is 0.3π.

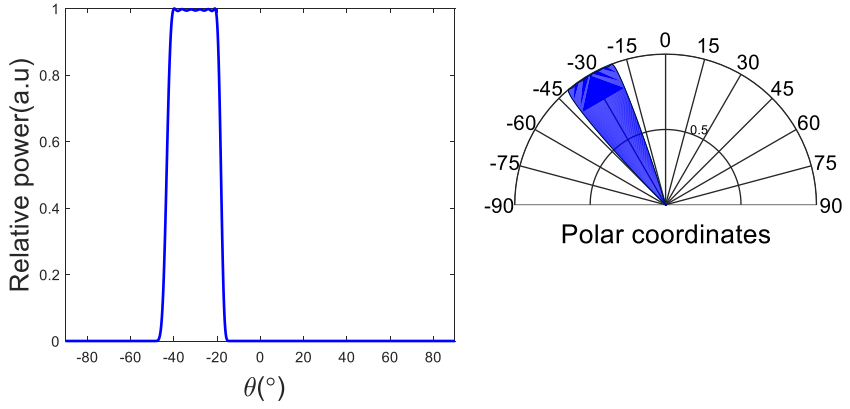

Fig. 7. The distribution when the center of the main lobe of the far field pattern points to −30°. The number of waveguides is 64, the distance between waveguides $d = 0.775$ μm, the window function is Kaiser window, and the cut-off frequency of the FIR filter is 0.3π.

dot product $\overrightarrow{R_n} \cdot \overrightarrow{r_e}$, which $\overrightarrow{R_n}$ is the vector from the origin to the nth element, $\overrightarrow{r_e}$ is the unit vector from the origin to the far-field point P. For any radiation element, its coordinate on the plane is (md_x, nd_y), it can be calculated from geometric relations that:

$$\overrightarrow{R_n} \cdot \overrightarrow{r_e} = md_x \sin\theta\cos\varphi + nd_y \sin\theta\sin\varphi \tag{16}$$

The derivation process can be extended from the one dimensional analysis to the two-dimensional case. Therefore, the far-field intensity distribution of two-dimensional optical phased array is expressed as follows:

$$E(\theta) = \sum_{m=0}^{M-1} \exp\left[jkmd_x\left(\sin\theta_s\cos\varphi_s - \sin\theta\cos\varphi\right)\right] \cdot \sum_{n=0}^{N-1} A_{mn} \exp\left[jknd_y\left(\sin\theta_s\sin\varphi_s - \sin\theta\sin\varphi\right)\right] \tag{17}$$

Among them, A_{mn} is the amplitude of the radiation element with the coordinate of $(md_x, nd_y, 0)$, θ and φ represent elevation and azimuth angles, θ_s is elevation angle of main beam direction of OPA, φ_s is

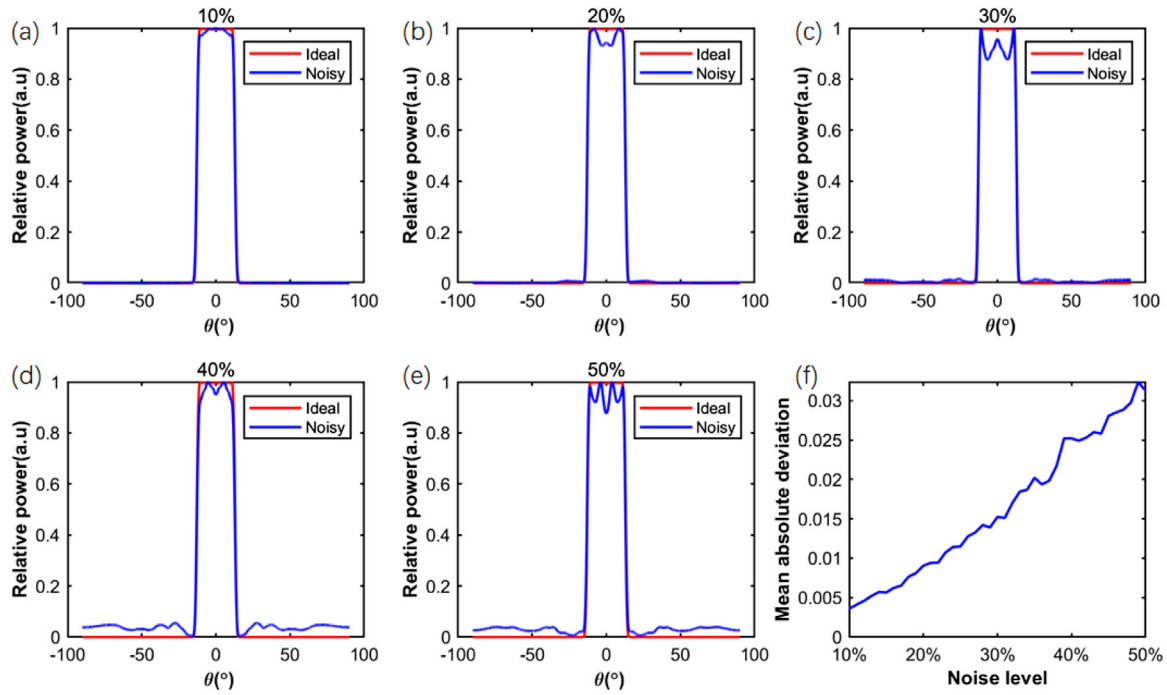

Fig. 8. (a)–(e) The far-fields obtained when noise in different levels is applied to the amplitude modulation sequence and the far-fields corresponding to the sequence without noise. (f) The mean absolute deviation between the corresponding far-field and the far-field without noise.

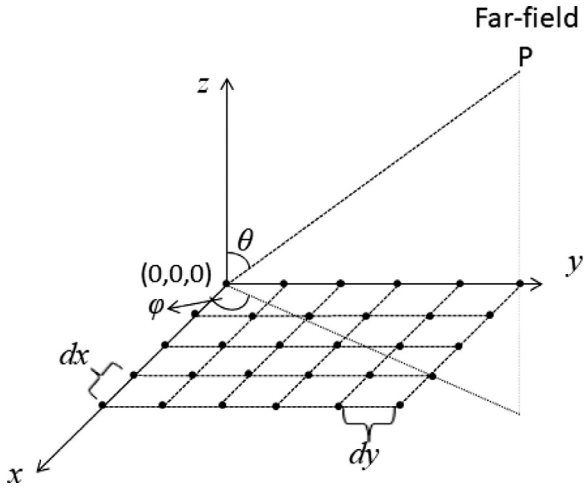

Fig. 9. Two-dimensional rectangular array optical phased array geometric model.

azimuth angle of main beam direction. The amplitude modulation of one dimensional optical phased array extends to two dimensional amplitude modulation, if the number of radiation elements in the x and y directions of the two-dimensional OPA is the same as N and the distance between waveguides in both directions is d, the amplitude of each radiation element is modulated. Assuming that the amplitude weighted sequence of the impulse response of the FIR digital filter designed by the window function is A_N, the weighted amplitude matrix is $A_{N\times N} = A_N^T A_N$ for the $N \times N$ two-dimensional OPA. The amplitude distribution of the two-dimensional case is shown in Fig. 10(a), the amplitude distribution is expanded to 2-D case by using the FIR digital filter impulse response sequence designed by Kaiser window. After weighted by the amplitude of the modulation matrix, the far-field intensity distribution is shown in Fig. 10(b). The far-field intensity distribution is similar to the rectangular distribution. It can be seen that the amplitude modulation of the one-dimensional OPA is also suitable for the two-dimensional OPA.

4. Amplitude correction considering single waveguide radiation pattern

In the above formulas, when calculating the far-field intensity distribution of the OPA, it is assumed that the radiation pattern $f(\theta)$ of each waveguide is equal and $f(\theta)$=1. Now we consider the situation of radiation pattern $f(\theta) \neq 1$, in this case, the far-field intensity distribution function of optical phased array is:

$$E(\theta) = f(\theta) \sum_{n=0}^{N-1} B(n) \exp\left(jnkd\left(\sin\theta_s - \sin\theta\right)\right) \tag{18}$$

If we still want to get the same far-field intensity distribution as before without considering the waveguide radiation pattern, that is:

$$\begin{aligned} E(\theta) &= f(\theta) \sum_{n=0}^{N-1} B(n) \exp\left(jnkd\left(\sin\theta_s - \sin\theta\right)\right) \\ &= \sum_{m=0}^{M-1} A(m) \exp\left(jmkd\left(\sin\theta_s - \sin\theta\right)\right) \end{aligned} \tag{19}$$

Let ω=kd(sinθ-sinθ_s), the above formula can be rewritten into:

$$E(\theta) = f(\omega) \sum_{n=0}^{N-1} B(n) \exp(-jn\omega) = \sum_{m=0}^{M-1} A(m) \exp(-jm\omega) \tag{20}$$

When calculating the far-field pattern of the optical phased array, the number of waveguides is finite, assume the number of waveguides is extended to infinite, and the waveguides are placed on both sides with the origin, then:

$$E(\theta) = f(\omega) \sum_{n=-\infty}^{\infty} B(n) \exp(-jn\omega) = \sum_{m=-\infty}^{\infty} A(m) \exp(-jm\omega) \tag{21}$$

$$\sum_{n=-\infty}^{\infty} B(n) \exp(-jn\omega) = \frac{1}{f(\omega)} \sum_{m=-\infty}^{\infty} A(m) \exp(-jm\omega) \tag{22}$$

$1/f(\omega)$ can be written as a discrete Fourier transform of an infinite sequence $g(q)$, that is:

$$\frac{1}{f(\omega)} = \sum_{q=-\infty}^{\infty} g(q) \exp(-jq\omega) \Rightarrow g(q) = \frac{1}{2\pi} \int_{-\pi}^{\pi} \frac{1}{f(\omega)} \exp(jq\omega)\, d\omega \tag{23}$$

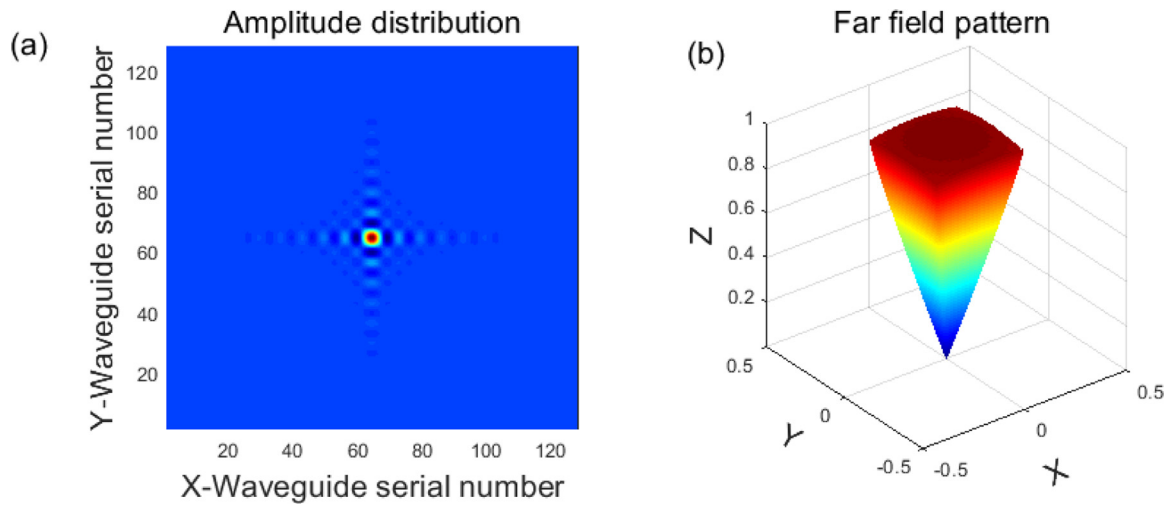

Fig. 10. (a) The sequence distribution of amplitude modulation for two-dimensional 128 × 128 OPA. The cut-off frequency of the FIR digital filter designed by Kaiser window is 0.3π, and the waveguide spacing in x and y directions is $d = 1$ μm. (b) The far-field pattern of two dimensional OPA modulated by the amplitude shown in (a).

Assuming that the radiation pattern belongs to the Gaussian distribution $f(\omega) \propto \exp(-\omega^2/\xi^2)$, $g(q)$ can be calculated by:

$$g(q) = \frac{1}{2\pi} \int_{-\pi}^{\pi} \exp\left(\frac{\omega^2}{\xi^2}\right) \exp(jq\omega)\, d\omega \tag{24}$$

Eq. (22) can be written as:

$$\sum_{n=-\infty}^{\infty} B(n) \exp(-jn\omega) = \sum_{q=-\infty}^{\infty} g(q) \exp(-jq\omega) \sum_{m=-\infty}^{\infty} A(m) \exp(-jm\omega) \tag{25}$$

Let $m = n - q$:

$$\begin{aligned} \sum_{n=-\infty}^{\infty} B(n) e^{-jn\omega} &= \sum_{q=-\infty}^{\infty} g(q) \\ &\quad \times \exp(-jq\omega) \sum_{n=-\infty}^{\infty} A(n-q) \exp(-j(n-q)\omega) \\ &= \sum_{n=-\infty}^{\infty} \left[\sum_{q=-\infty}^{\infty} g(q) \cdot A(n-q) \right] \exp(-jn\omega) \end{aligned} \tag{26}$$

The amplitude sequence which is required to obtain the same far-field intensity distribution as the previous amplitude modulation can be calculated by the following formula when considering the radiation pattern of each waveguide:

$$B(n) = \sum_{q=-\infty}^{\infty} g(q) \cdot A(n-q) \tag{27}$$

The above deduction is based on the assumption that the number of waveguides is infinite. But in practice, the number of waveguide elements is limited. When the number of waveguides is N and the value of $B(n)$ is calculated by formula (26), the length of $B(n)$ sequence is $2N-1$, we intercept the N values from the center of the sequence as sequence $B(n)$. Fig. 11 shows the amplitude distribution of sequences $B(n)$ and $A(n)$. Input $B(n)$ into formulate (19) and get the far-field pattern under the radiation pattern of the waveguide is considered, it can be seen from Fig. 11(b) that the calculated far-field intensity fluctuates greatly in this case, which is due to the fact that the number of waveguides cannot be infinite, so the calculated sequence $B(n)$ has some errors. From the previous analysis, we can see that the amplitude sequence weighted by window functions can greatly weaken the far-field intensity fluctuation, so we consider using Kaiser window to weigh the calculated amplitude distribution $B(n)$ to get a new amplitude sequence $B(n)\omega(n)$, the OPA is modulated by this new sequence, and the far-field pattern is shown in Fig. 11(c). It can be seen that the fluctuation of the far-field intensity distribution obtained by the new sequence modulation is greatly weakened, and it is basically the same as that obtained far-field pattern without considering the radiation pattern. From the above analysis, we can get the ideal uniform rectangular far-field intensity distribution by weighting the amplitude sequence with the window functions when considering the radiation pattern of the waveguide. This proves that the method of weighting the amplitude sequence with the window functions is feasible in practice.

5. Conclusion

In this paper, a method of amplitude modulation for small spacing uniform optical phased array is presented. The impulse response sequence of FIR digital filter designed by window functions is used to weigh the amplitude of the OPA. The uniform rectangular distribution of far-field intensity is achieved, and this method can be extended to two-dimensional rectangular planar OPA. Finally, the amplitude modulation sequence is corrected when considering the waveguide radiation pattern, and get the far-field intensity distribution which is similar to that without considering the waveguide radiation pattern, which proves the feasibility of this method in practice. We have successfully proved a new method, which is using optical phased array to solve the problem of non-uniform far-field distribution of Flash Lidar.

Funding

This work is supported by the Funding. National Natural Science Foundation of China under Grants No. 62090054 No. 61627820, No. 61934003; Jilin Scientific and Technological Development Program, China (20200501007GX); Program for JLU Science and Technology Innovative Research Team, China (JLUSTIRT, 2021TD-39)

Declaration of competing interest

The authors declare that they have no known competing financial interests or personal relationships that could have appeared to influence the work reported in this paper.

Appendix A. Supplementary data

Supplementary material related to this article can be found online at https://doi.org/10.1016/j.optcom.2021.127661.

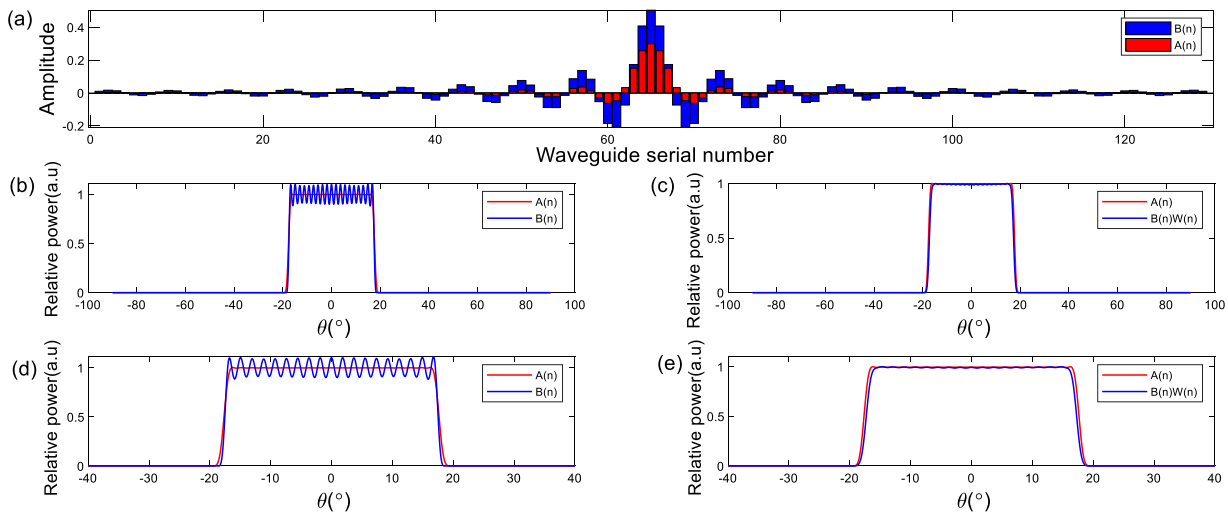

Fig. 11. (a) The comparison of the two amplitude modulation sequences $A(n)$ and $B(n)$ corresponding to whether the waveguide radiation pattern is taken into account or not when the same far-field intensity distribution is obtained. The number of waveguides $N = 129$, the distance between waveguides $d = 0.775$ μm, the cut-off frequency of the FIR filter is 0.3π, and the window function is Kaiser window. (b) The comparison of far-field pattern after modulated by $A(n)$ and $B(n)$, (d) is the enlargement of (b). (c) The comparison of far-field pattern after modulated by $A(n)$ and $B(n)\omega(n)$. (e) is the enlargement of (c).

References

[1] J. Busck, H. Heiselberg, Gated viewing and high-accuracy three-dimensional laser radar, Appl. Opt. 43 (24) (2004) 4705–4710.

[2] H.V. Duong, M.A. Lefsky, T. Ramond, C. Weimer, The electronically steerable flash lidar: A full waveform scanning system for topographic and ecosystem structure applications, IEEE T. Geosci. Remote sens. 50 (11) (2012) 4809–4820.

[3] P. Zhang, X. Du, J. Zhao, Y. Song, H. Chen, High resolution flash three-dimensional LIDAR systems based on polarization modulation, Appl. Opt. 56 (13) (2017) 3889–3894.

[4] S.W. Hutchings, N. Johnston, I. Gyongy, T. Al Abbas, N.A.W. Dutton, M. Tyler, S. Chan, J. Leach, R.K. Henderson, A reconfigurable 3-D-stacked SPAD imager with in-pixel histogramming for flash LIDAR or high-speed time-of-flight imaging, IEEE J. Solid-State Circuits 54 (11) (2019) 2947–2956.

[5] B. Javidi, A. Bulyshev, J.-Y. Son, D. Pierrottet, F. Amzajerdian, M. Martinez-Corral, F. Okano, G. Busch, M. Vanek, W. Osten, R. Reisse, Processing of three-dimensional flash lidar terrain images generating from an airborne platform, Proc. SPIE - Int. Soc. Opt. Eng. 7329 (2009) 73290I-73290I-9.

[6] C. Corner, H. Simonds, J. Dickson, A.M. Rojas, A super-resolution algorithm for enhancement of FLASH LIDAR data, Proc. SPIE - Int. Soc. Opt. Eng. 9020 (2013) 90200B.

[7] Andrew E. Johnson, Jason A. Keim, T. Ivanov, Analysis of flash lidar field test data for safe lunar landing, in: 2010 IEEE Aerospace Conference, 2010, pp. 1-11.

[8] C.-I.C.a.R. Stettner, Drogue tracking using 3D flash LIDAR for autonomous aerial refueling, Proc. SPIE - Int. Soc. Opt. Eng. 8037 (2011) 80370Q.

[9] B.C.R.A. Gelbart, R.S. Light, C.A. Schwartzlow, A.J. Griffis, Flash lidar based on multiple-slit streak tube imaging lidar, Laser Radar Technol. Appl. (2002) 9–18.

[10] G. Zhou, J. Yang, X. Li, X. Yang, Advances of flash LIDAR development onboard UAV, in: ISPRS - International Archives of the Photogrammetry, 2012, pp. 193-198.

[11] J. Sun, J. Liu, Q. Wang, A multiple-slit streak tube imaging lidar and its detection ability analysis by flash lidar equation, Optik 124 (3) (2013) 204–208.

[12] V.A. Karel, B. Wim, J. Jana, L.T. Nicolas, H. Romuald, B. Roel, Off-chip beam steering with a one-dimensional optical phased array on silicon-on-insulator, Opt. Lett. 34 (9) (2009) 1477–1479.

[13] K. Van Acoleyen, K. Komorowska, W. Bogaerts, R. Baets, One-dimensional off-chip beam steering and shaping using optical phased arrays on silicon-on-insulator, J. Lightwave Technol. 29 (23) (2011) 3500–3505.

[14] V.A. Karel, R. Hendrik, B. Roel, Two-dimensional optical phased array antenna on silicon-on-insulator, Opt. Express 18 (13) (2010) 13655–13660.

[15] J.K. Doylend, M.J.R. Heck, J.T. Bovington, J.D. Peters, L.A. Coldren, J.E. Bowers, Two-dimensional free-space beam steering with an optical phased array on silicon-on-insulator, Opt. Express 19 (22) (2011) 21595–21604.

[16] K. Van Acoleyen, W. Bogaerts, R. Baets, Two-dimensional dispersive off-chip beam scanner fabricated on silicon-on-insulator, IEEE Photonics Technol. Lett. 23 (17) (2011) 1270–1272.

[17] J. Sun, E. Timurdogan, A. Yaacobi, E.S. Hosseini, M.R. Watts, Large-scale nanophotonic phased array, Nature 493 (7431) (2013) 195–199.

[18] J.K. Doylend, M.J.R. Heck, J.T. Bovington, J.D. Peters, M.L. Davenport, L.A. Coldren, J.E. Bowers, Hybrid III/V silicon photonic source with integrated 1D free-space beam steering, Opt. Lett. 37 (20) (2012) 4257–4259.

[19] H. Abediasl, H. Hashemi, Monolithic optical phased-array transceiver in a standard SOI CMOS process, Opt. Express 23 (5) (2015) 6509–6519.

[20] L. Zhang, Y. Li, M. Tao, Y. Wang, Y. Hou, B. Chen, Y. Li, L. Qin, F. Gao, X. Luo, G. Lo, J. Song, Large-scale integrated multi-lines optical phased array chip, IEEE Photon. J. 12 (4) (2020) 1–8.

[21] D. Kwong, A. Hosseini, J. Covey, Y. Zhang, X. Xu, H. Subbaraman, R.T. Chen, On-chip silicon optical phased array for two-dimensional beam steering, Opt. Lett. 39 (4) (2014) 941–944.

[22] T. Komljenovic, P. Pintus, On-chip calibration and control of optical phased arrays, Opt. Express 26 (3) (2018) 3199–3210.

[23] L. Zhang, Y. Li, Y. Hou, Y. Wang, M. Tao, B. Chen, Q. Na, Y. Li, Z. Zhi, X. Liu, X. Li, F. Gao, X. Luo, G.-Q. Lo, J. Song, Investigation and demonstration of a high-power handling and large-range steering optical phased array chip, Opt. Express 29 (19) (2021) 29755–29765.

[24] J. Sun, E. Hosseini, A. Yaacobi, D.B. Cole, G. Leake, D. Coolbaugh, M.R. Watts, Two-dimensional apodized silicon photonic phased arrays, Opt. Lett. 39 (2) (2014) 367–370.

[25] A.V. Oppenheim, R.W. Schafer, J.R. Buck, Discrete-Time Signal Processing, second ed., Prentice-Hall, Inc., 1999.

[26] M.G. Shayesteh, M. Mottaghi-Kashtiban, FIR filter design using a new window function, in: International Conference on Digital Signal Processing, 2009, pp. 1-6.